Supplementary Table 1. Cryo-EM data collection and refinement statistics.

BG505 SOSIP.664 in complex with 17b Fab and CJF-III-288	
EMDB	EMD-45530
PDB	9CF5
Data Collection and Processing	
Microscope	FEI TITAN KRIOS G1
Voltage (kV)	300
Detector	Gatan K3
Energy filter (slit)	Yes (20 eV)
Cs corrector	No
Magnification	105,000 x
Pixel Size (Å/px)	0.832 (0.416 superres)
Total electron dose ($e^-/Å^2$)	54.2
Dose rate (e^-/px/s)	15
Defocus Range (μm)	0.5-2.7
Micrograph collected	9,431
Number of picked particles	6,768,076
Box size (pix)	400
Number of final particles	1,087,694
Symmetry	C1
Resolution (Å) (FSC 0.143)	3.5
B-factor for map ($Å^2$)	159.5
Refinement (Phenix) & validation	
Model composition	
Non-hydrogen atoms	18,048
Protein	17,083
Ligands (CJF-III-288)	111
Average B-factors ($Å^2$)	
Protein	101
Ligands (CJF-III-288)	54
CC_mask	0.738
EMRinger Score	1.04
RMSD Bond lengths (Å)	0.004
RMSD Bond angles (°)	0.685
Molprobity score	2.17
Clash score	15.2
Rotamer outliers (%)	0.53
Ramachandran Plot	
Favored (%)	92.2
Allowed (%)	7.8
Disallowed (%)	0

Supplementary Table 2. CryoET data collection and refinement statistics

HIV_{BaL} virions in complex with 17b and CJF-III-288	
EMDB	46646
CryoET Collection and Data Processing	
Microscope	FEI Titan Krios
Voltage (kV)	300
Detector	Gatan K3
Energy Filter (slit)	Gatan Imaging Filter (20 eV)
Magnification	64,000 x
Pixel Size (Å/px)	1.346 (0.643 superres)
Total electron dose ($e^-/Å^2$)	119
Dose per image(tilt) ($e^-/Å^2$)	2.9
Number of Tilts	41
Tilt Increment	3°
Tilt Range	-60°-60°
Collection Scheme	Dose Symmetric
Volta Phase Plate	Yes
Defocus (μm)	0.5
Number of Tomograms Collected	87
Particles Picked	9419
Number of Final Particles	3507
Symmetry Applied	C1
B-factor Applied	-100
Resolution (Å) (FSC 0.143)	21.5

Supplementary Table 3. Demographic characterization of HIV-negative individuals from whom CD4 T cells were isolated and used for *in vitro* infection experiments

Donor	Age (years)	Sex
1	45	Male
2	53	Male
3	63	Male
4	45	Female
5	66	Male
6	38	Male
7	31	Male

Supplementary Table 4. Demographic characterization of ART-treated PLWH whose endogenously infected CD4 T cells were expanded *ex vivo*

Donor	Age (years)	Sex	Time since acquisition (years)	Time since ART initiation (years)	Plasma viral load
ART-1	44	Male	14	3	Undetectable
ART-2	53	Male	28	13	Undetectable
ART-3	58	Male	18	12	Undetectable
ART-4	59	Male	34	2	Undetectable

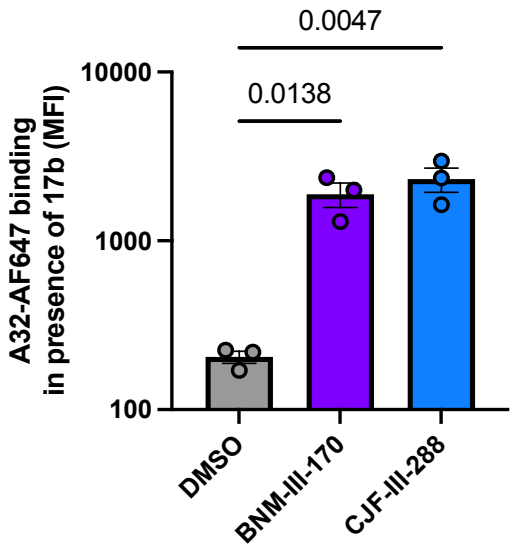

Supplementary Figure 1. CJF-III-288 and 17b combination enable recognition of HIV-1-infected cells by A32
Recognition of HIV-$1_{CH058TF}$-infected primary CD4+ T cells by Alexa-Fluor-647 conjugated A32 in combination with 17b and DMSO, BNM-III-170 or CJF-III-288. Graphs represent the median fluorescence intensities (MFI) obtained in 3 independent experiments. Data are presented as mean values +/- SEM.Statistical significance was tested using One-way ANOVA test with a Tukey post-test. P values are shown in the graph. Source data are provided as a Source Data file.

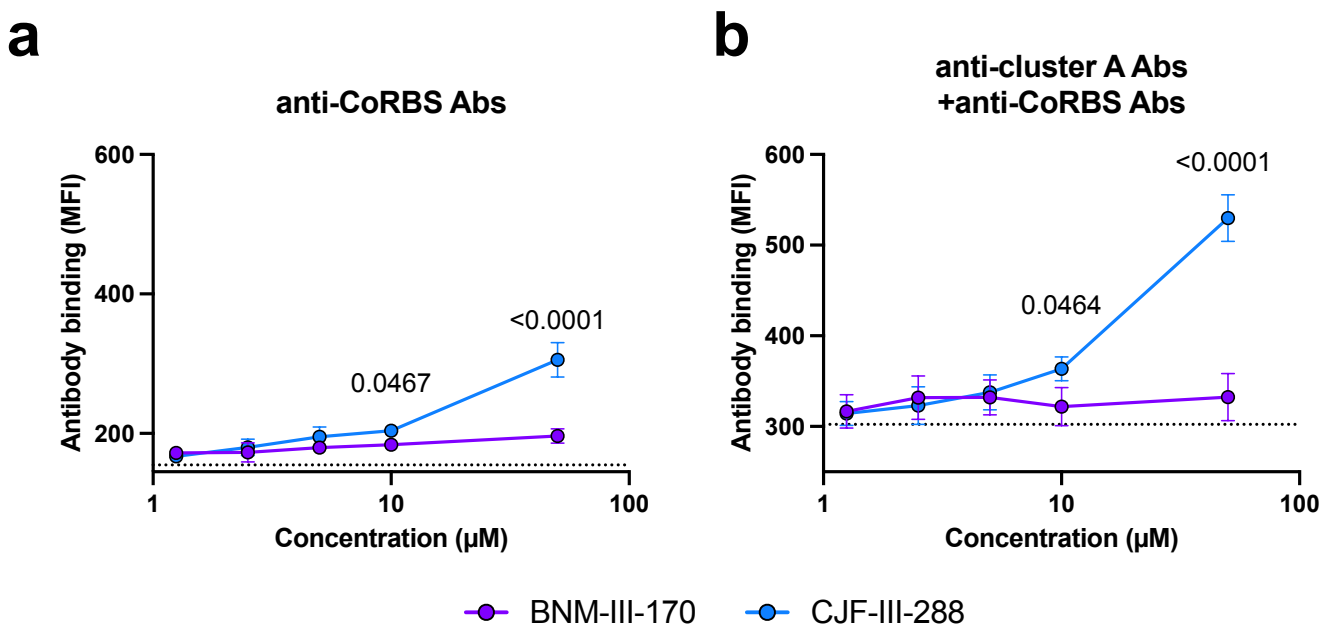

Supplementary Figure 2. Improved recognition of HIV-1_{BG505}-infected cells by nnAbs in presence of CJF-III-288. Recognition of HIV-1_{BG505}-infected primary CD4+ T cells by anti-CoRBS Abs **a**, alone or **b**, in combination with anti-cluster A Abs, in the presence of indicated concentration of BNM-III-170 or CJF-III-288. Graphs represent the median fluorescence intensities (MFI) obtained in 4 independent experiments. The dashed lines represent the mean binding obtained in absence of CD4mc.Data are presented as mean values +/- SEM. Statistical significance was tested using Two-way ANOVA test with a Holm-Sidak post-test. P values are shown in the graphs. Source data are provided as a Source Data file

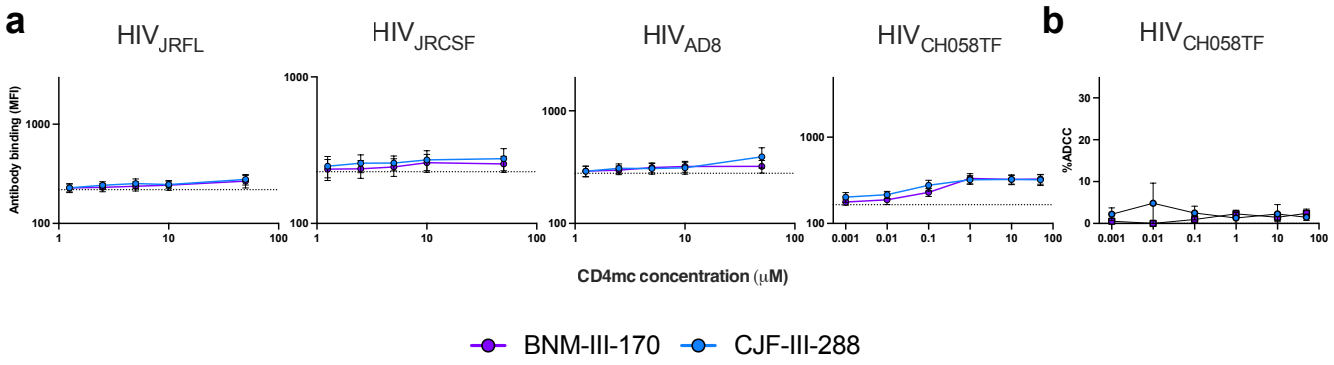

Supplementary Figure 3. A32 binding and ADCC activity in presence of different concentrations of CD4mc.
a, Recognition of primary CD4+ T cells infected with indicated IMC by the anti-cluster A Abs A32 in the presence of indicated concentration of BNM-III-170 or CJF-III-288. Graphs represent the median fluorescence intensities (MFI) obtained in at least 4 biological replicates with each IMCs (HIV-$1_{CH058TF}$ n=5, HIV-1_{JRFL} n=4, HIV-1_{AD8} n=4, HIV-1_{JRCSF} n=4). with each IMCs. **b**, ADCC-mediated elimination of CD4+ T cells infected HIV-$1_{CH058TF}$ by A32 in the presence of indicated concentration of BNM-III-170 or CJF-III-288. Shown are percentage of ADCC obtained in 3 biological replicates. Data are presented as mean values +/- SEM The dashed lines represent the mean binding or ADCC obtained in absence of CD4mc. Source data are provided as a Source Data file

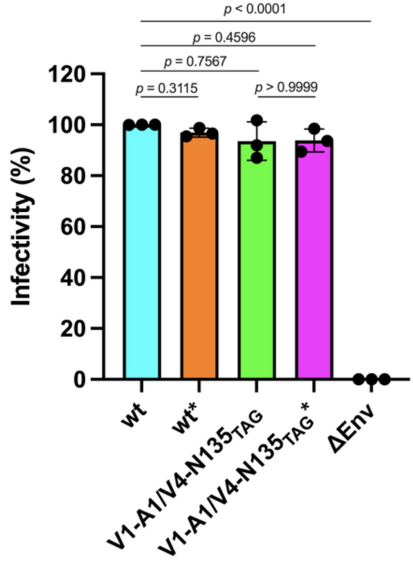

Supplemental Figure 4. Modifications to Env, including attachment of fluorophores, does not affect infectivity. Pseudovirus infectivity was measured using a luciferase assay. Infectivity is indicated for pseudovirions prepared with wild-type Env (wt); wt Env mock labeled with Cy3 and LD650 fluorophores (wt*); modified, unlabeled Env (V1-A1/V4-N135TAG); modified Env labeled with Cy3 and LD650 fluorophores (V1-A1/V4-N135TAG*); and particles lacking Env (DEnv). Data are presented normalized to wt and background subtracted. Each point indicates the arithmetic mean of three technical replicates. Bars represent the average of three independent experiments per condition. Error bars reflect the standard error. p-values were determined using a one-way ANOVA. Source data are provided as a Source Data file

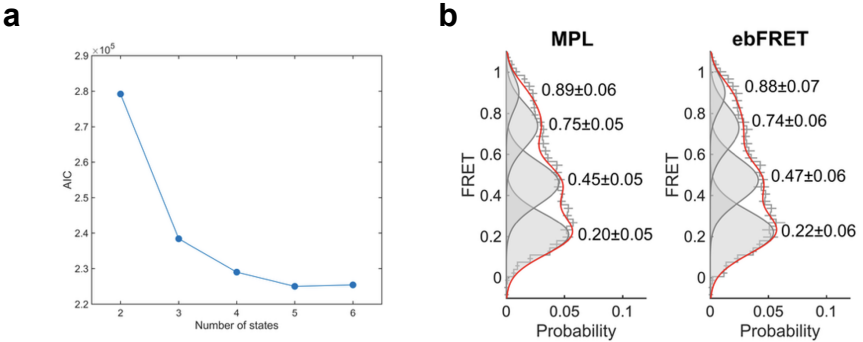

Supplemental Figure 5. Model selection for kinetic analysis of smFRET data.
a, Five different models were considered during HMM analysis of the smFRET trajectories. Model parameters were optimized by maximization of likelihood using the MPL algorithm. Model fitness was compared by correcting the maximized likelihood for different numbers of model parameters using the Akaike information criterium (AIC). Minimization of the AIC indicates the model that best represents the data. Based on this criterium, the 5-state model (4 non-zero FRET states, and a 0-FRET state) was selected. Addition of a sixth state did not improve model fitness. **b**, FRET histograms with Gaussian fits of the modeled FRET states, presented as in Fig. 6. (Left) FRET states are indicated as determined through fitting the 5-state model (0 FRET is omitted for clarity) using MPL. (Right) The same data fit using ebFRET, which requires no prior assumptions about the FRET values. The mean FRET values standard deviations determined through both methods of HMM analysis are indicated

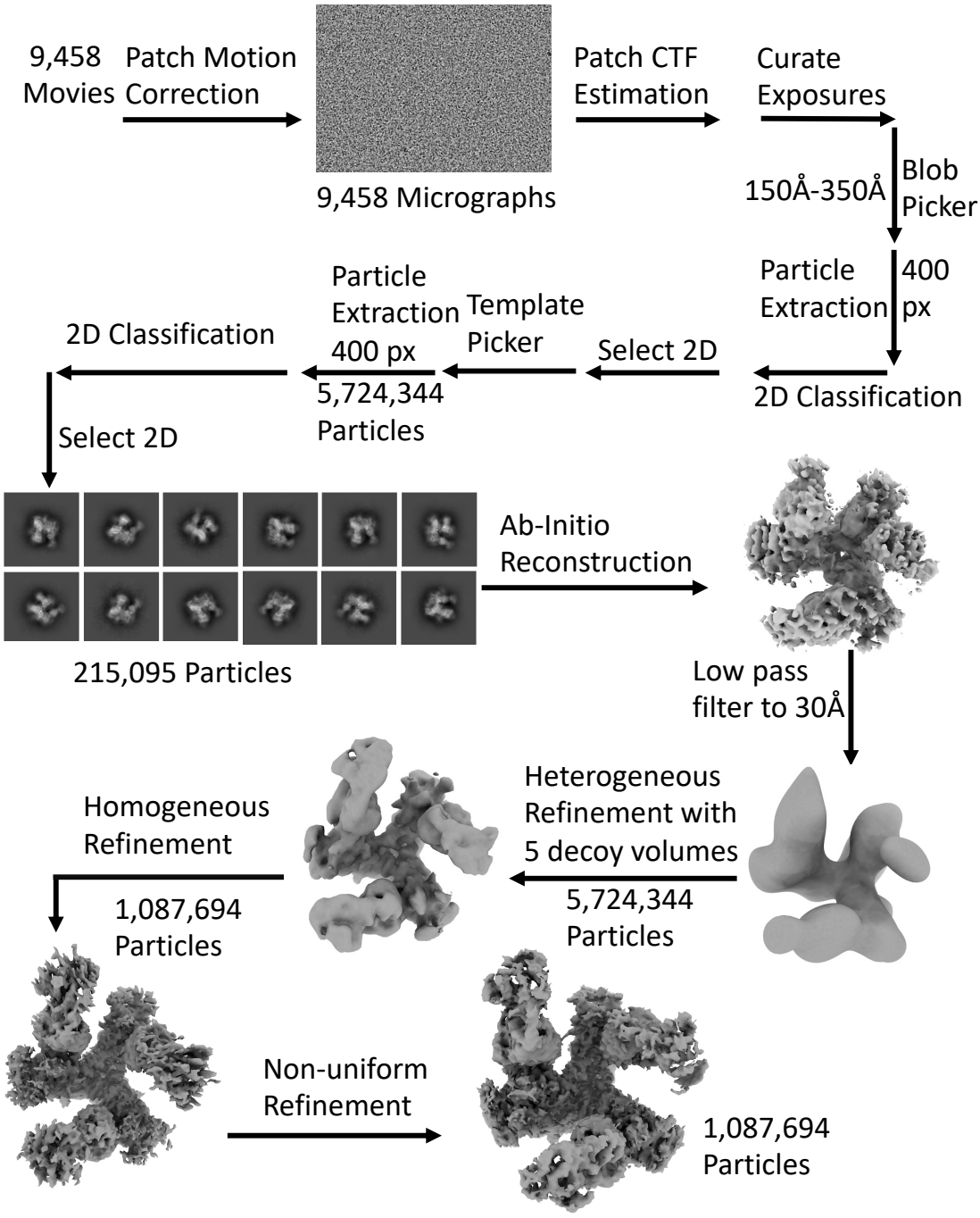

Supplementary Figure 6. CryoEM data processing workflow.
Flowchart diagram showing the steps required to convert the raw movie data into a high-resolution structure by single-particle cryo-EM. Raw movie data was first aligned to correct beam induced motion (Patch Motion Corroection in CryoSparc) and then an estimate of the contrast transfer function (CTF) was made with Patch CTF estimation in CryoSparc. Particles were initially picked by a blob-based algorithm (Blob Picker in CryoSparc), 2D classes were generated, and good 2D classes were used as templates for a template-based particle picking algorithm (Template Picker). After Template Picker, 215,095 particles with well-balanced orientations were used for Ab Initio reconstruction. All Template Picked particles were then subjected to heterogeneous refinement with five decoy volumes and the low pass filtered Ab Initio map. This was repeated several times. The final reconstruction was obtained after homogeneous and non-uniform refinement of the heterogeneous refined map.

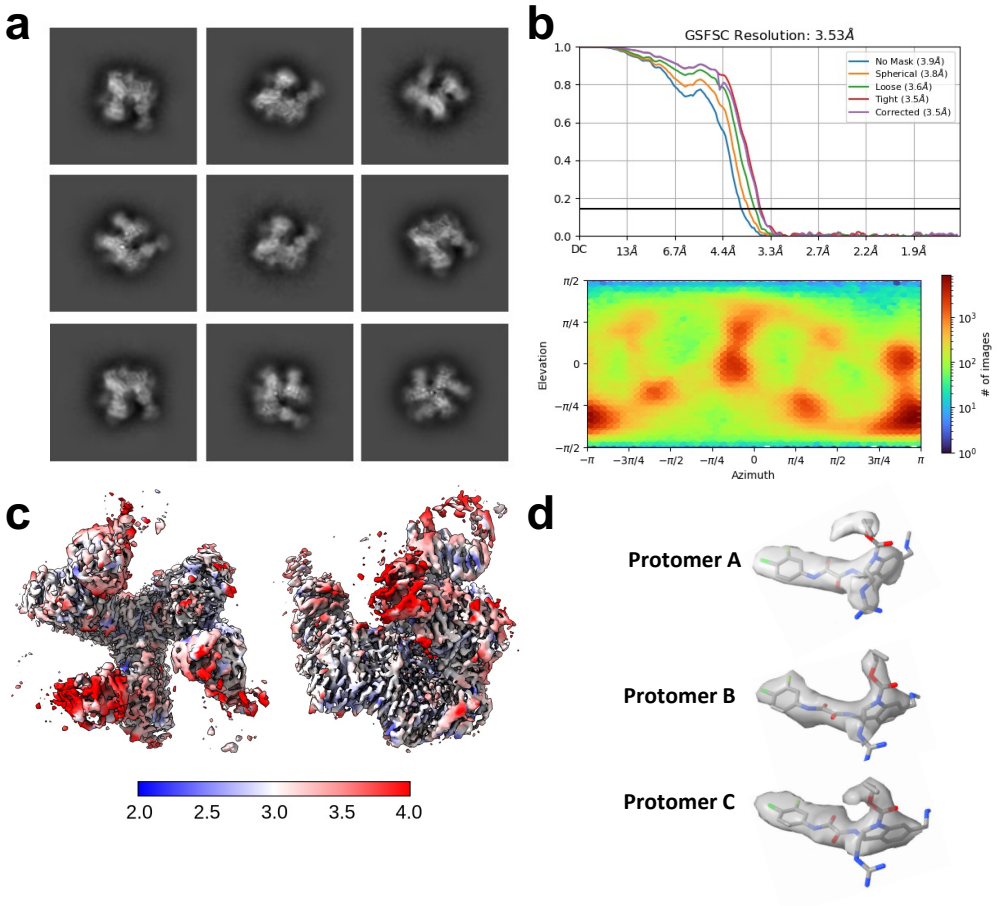

Supplementary Figure 7. Cryo-EM structure of the CJF-III-288-BG505 SOSIP.664-17b Fab complex.
a, Selected 2D classes for ab initio map reconstruction. Micrographs were collected using on a FEI Titan Krios electron microscope operating at 300 kV equipped with Gatan Bioquantum Image filter-K3 direct electron detector (Gatan Inc). **b**, The Fourier shell correlation curves (FSC cutoff 0.143) from the final non-uniform refinement step and the direction distribution plot of all particles used in the final refinement. **c**, Local resolution estimation. **d**, Density and corresponding model for CJF-III-288 from each protomer (protomer A corresponds to chain C, protomer B corresponds to chain A and protomer C corresponds to chain E).

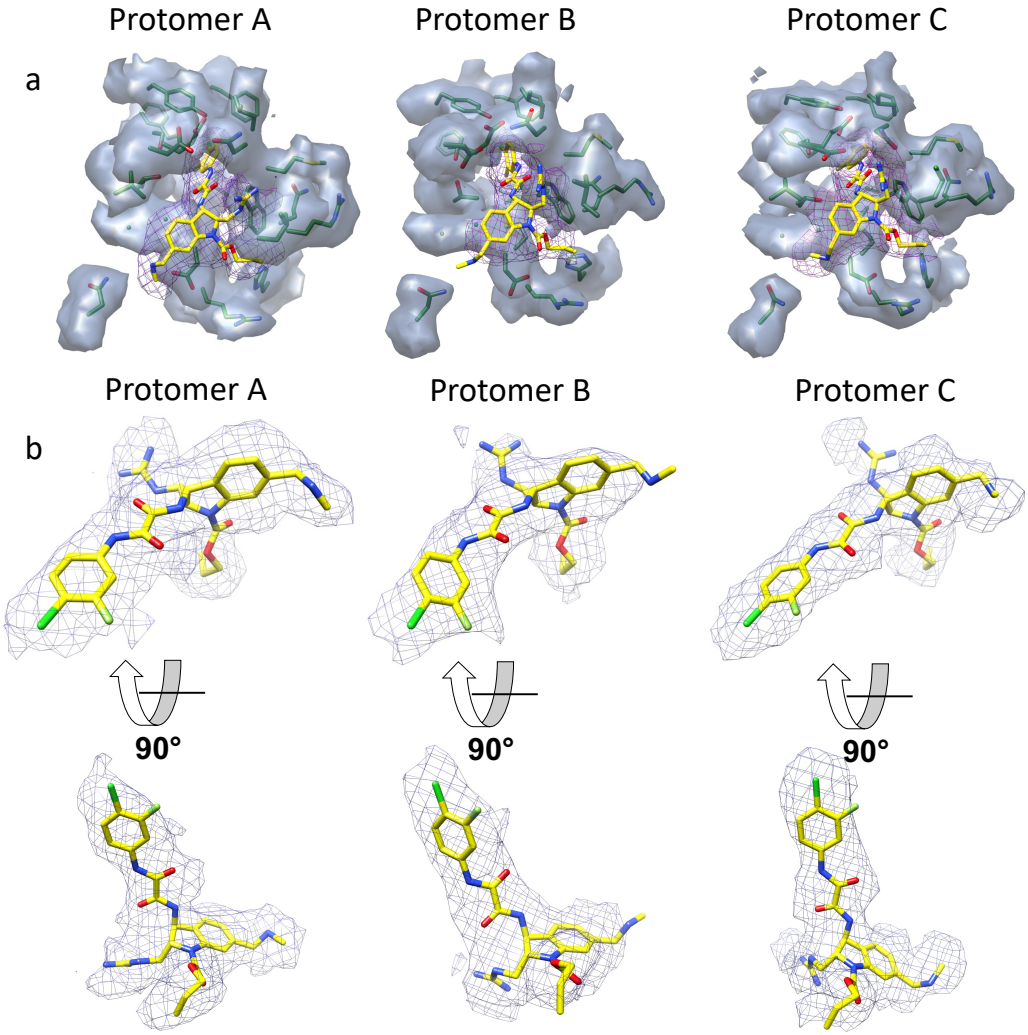

Supplementary Figure 8. Fit into map of CJF-III-288 and binding site residues.
a. CJF-III-288 from each of the three protomers are shown as yellow sticks and binding site residues are shown as green sticks. The map surrounding residues that form the binding site and CJF-III-288 are shown at the same contour level for each protomer, 0.06. The portion of the map covering binding site residues is shown as a surface and the portion of the map covering CJF-III-288 is shown as mesh. **b**. two orthogonal views of CJF-III-288 from each protomer shown after removing binding site residues.

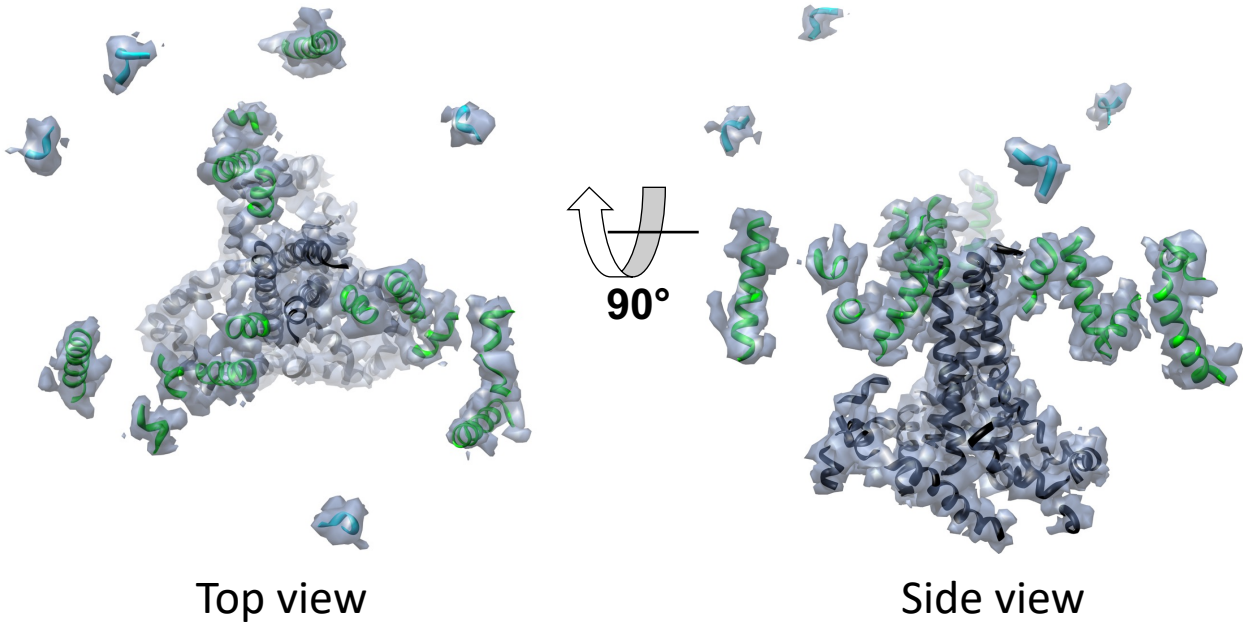

Supplementary Figure 9. Individual helices are shown with the superimposed structural model.
Side and top views of the trimer. Helices from gp120 are shown as green ribbons, helices from gp41 as grey ribbons, and helices from 17b as cyan ribbons. The map is shown as a grey surface at a contour level of 0.06.

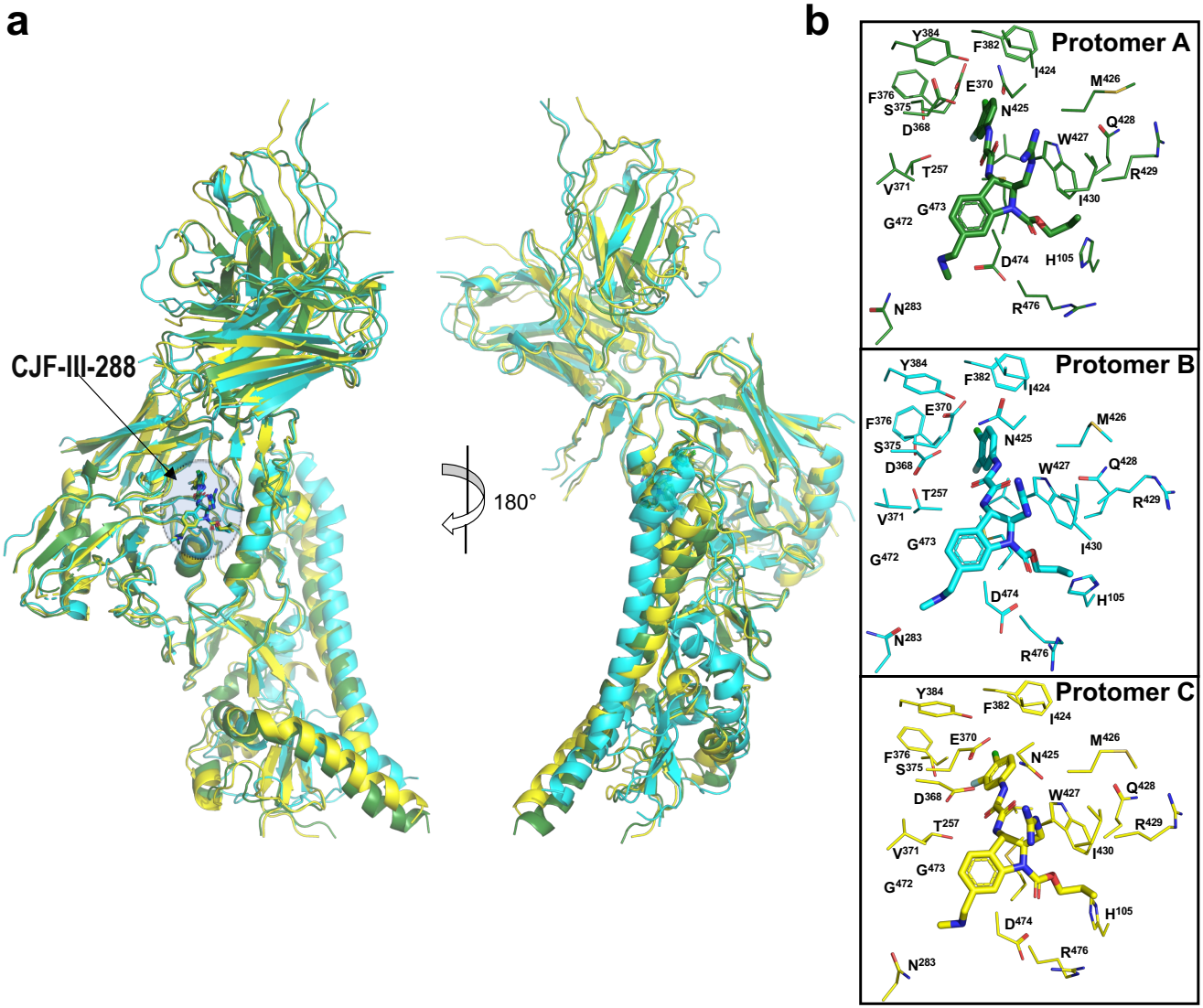

Supplementary Figure 10. Superimposition of the three protomers of the asymmetric trimer of the CJF-III-288-BG505-17b Fab complex
a, Superimposition of protomers. 17b, gp120 and gp41 in each protomer are shown as cartoons and CJF-III-288 is shown as sticks. Protomer A is colored green, protomer B colored cyan and protomer C colored yellow. The protomers were superimposed and the root-mean-square deviation (RMSD) values of Cα atoms between protomers calculated. The RMSD between protomers A and B, protomers A and C, and protomers B and C are 2.7 Å, 1.73 Å, 3.14 Å, respectively. **b**, Residues forming the binding pockets in each protomer. The RMSD values of Cα atoms of pocket residues are 0.565 Å, 0.563 Å, 0.524 Å for protomers A and B, protomers A and C, and protomers B and C, respectively.

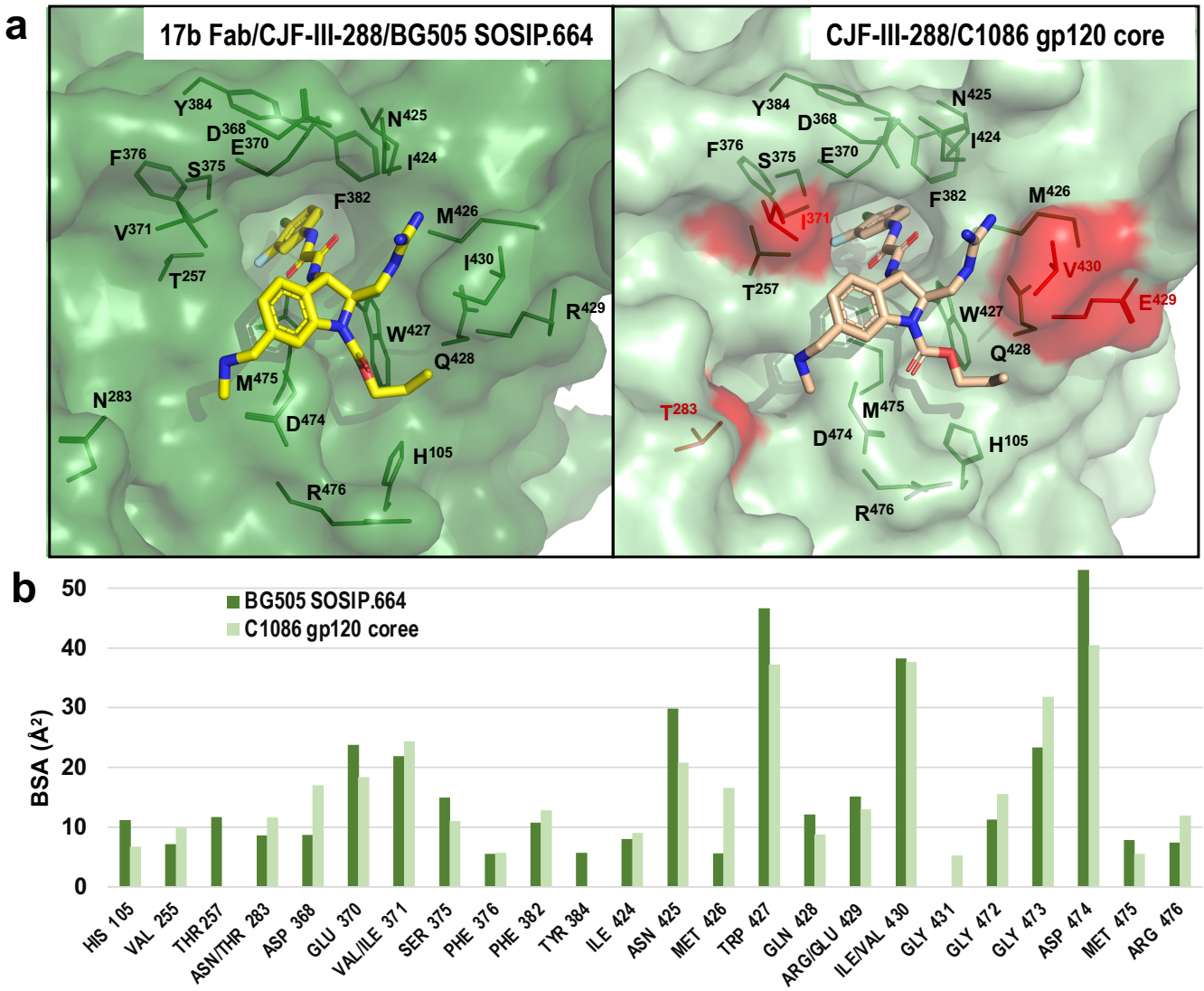

Supplementary Figure 11. Comparison of the CJF-III-288 binding pockets as in the CJF-III-288-BG505-17b Fab and the CJF-III-288-C1086 gp120 core$_e$ complexes.

a, The CJF-III-170 binding pocket (from Protomer A) is superimposed based upon gp120 to the complex of the CJF-III-288 gp20 coree (8FM3) . Strain specific residues in CJF-III-288-gp120 coree complex are highlighted red. **b**, Buried surface area (BSA) of gp120 residues buried at the CJF-III-288 binding interfaces. Source data of **b** are provided as a Source Data file

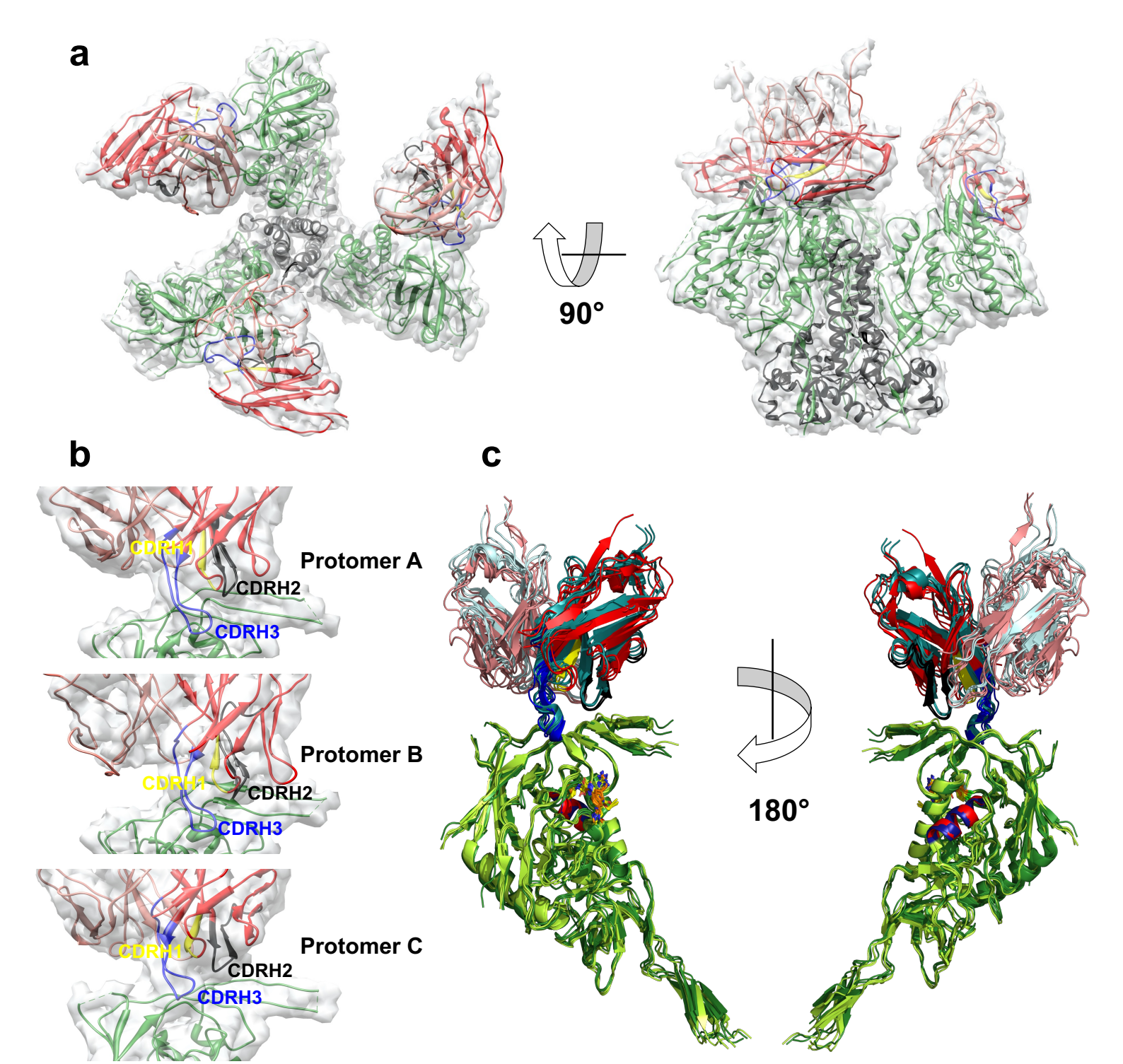

Supplementary Figure 12. Details of 17b interaction with SOSIP.664 trimer and individual gp120 subunits. a, Fitting of the CJF-III-288-BG505 SOSIP.664-17b model into the experimental Cryo-EM reconstruction. Top and side views are shown. In the complex model, gp41 is depicted as a dark grey cartoon, gp120 as dark green, the 17b heavy chain variable domain as red, and the 17b light chain variable domain as salmon. The 17b CDRs are highlighted, with CDR H1 in yellow, CDR H2 in black, and CDR H3 in blue. The density map is displayed as a transparent grey surface, with the contour level set to 0.042 and a 2 Å mask around the model was applied. **b**, A close-up view of the 17b-gp120 interface in protomers A, B, and C from panela a. Heavy chain CDRs are as labeled. **c**, Alignment (based on the gp120 molecule) of individual gp120-17b Fab dimers from the CJF-III-288-BG505 SOSIP.664-17b and BNM-III-170-BG505 structures. CJF-III-288 is represented as yellow sticks, while BNM-III-170 is shown as orange sticks. The remaining portions are shown as cartoons. The color scheme for the three protomers in the CJF-III-288-BG505 SOSIP.664-17b complex matches panel a, while the BNM-III-170-BG505 SOSIP.664-17b protomers are colored light green for gp120 and dark and light cyan for the 17b Fab. The α0 helices are highlighted in red and blue in the CJF-III-170 and BNM-III-170 complexes, respectively.

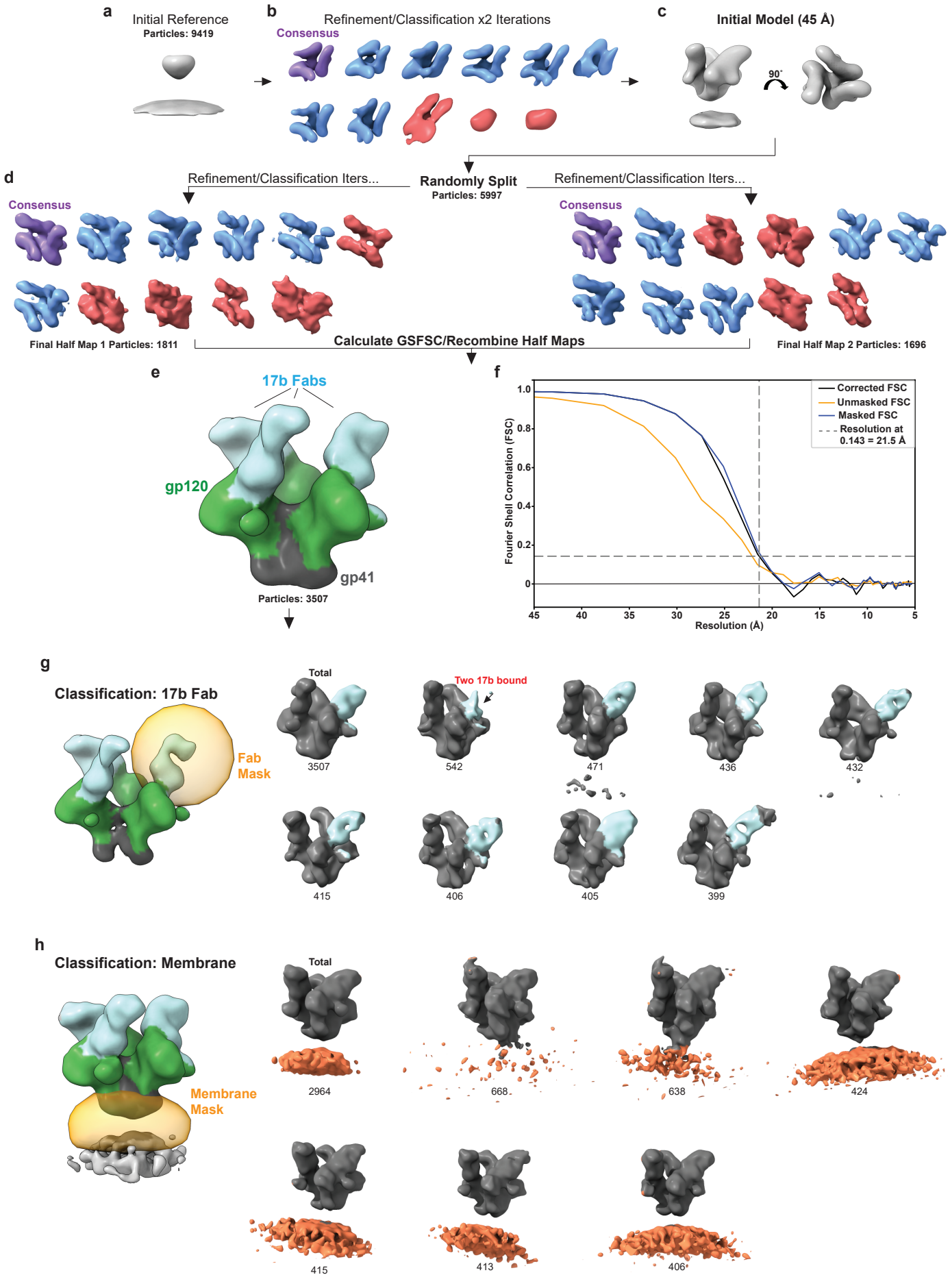

Supplementary Figure 13. CryoET refinement and classification workflow.
a, HIV-1BaL Env trimers in complex with CJF-III-288 and 17b Abs, along with the center of each virion, were manually picked using IMOD software. PEET program spikeInit was used to determine approximate particle orientations to generate an initial reference. **b,c**, Refinement and classification were performed to remove junk particles (red) and generate an initial model. Resolution was limited to 45 Å by strong lowpass filtration and binning. **d**, Particles were randomly split into two halves for further refinement. Classification was performed to select Env trimers bound to three 17b Abs (blue). **e**, Isosurface rendering of the structure. **f**, Fourier shell correlation calculated from the two half-maps. Resolution was estimated at FSC = 0.143. **g**, Masked classification of the 17b Fab domain with weaker density shows heterogeneity in the 17b position. **h**, Masked classification on the membrane for Env bound to three 17b shows tilting on the membrane. The number of particles in each subclass for **g** and **h** are shown.

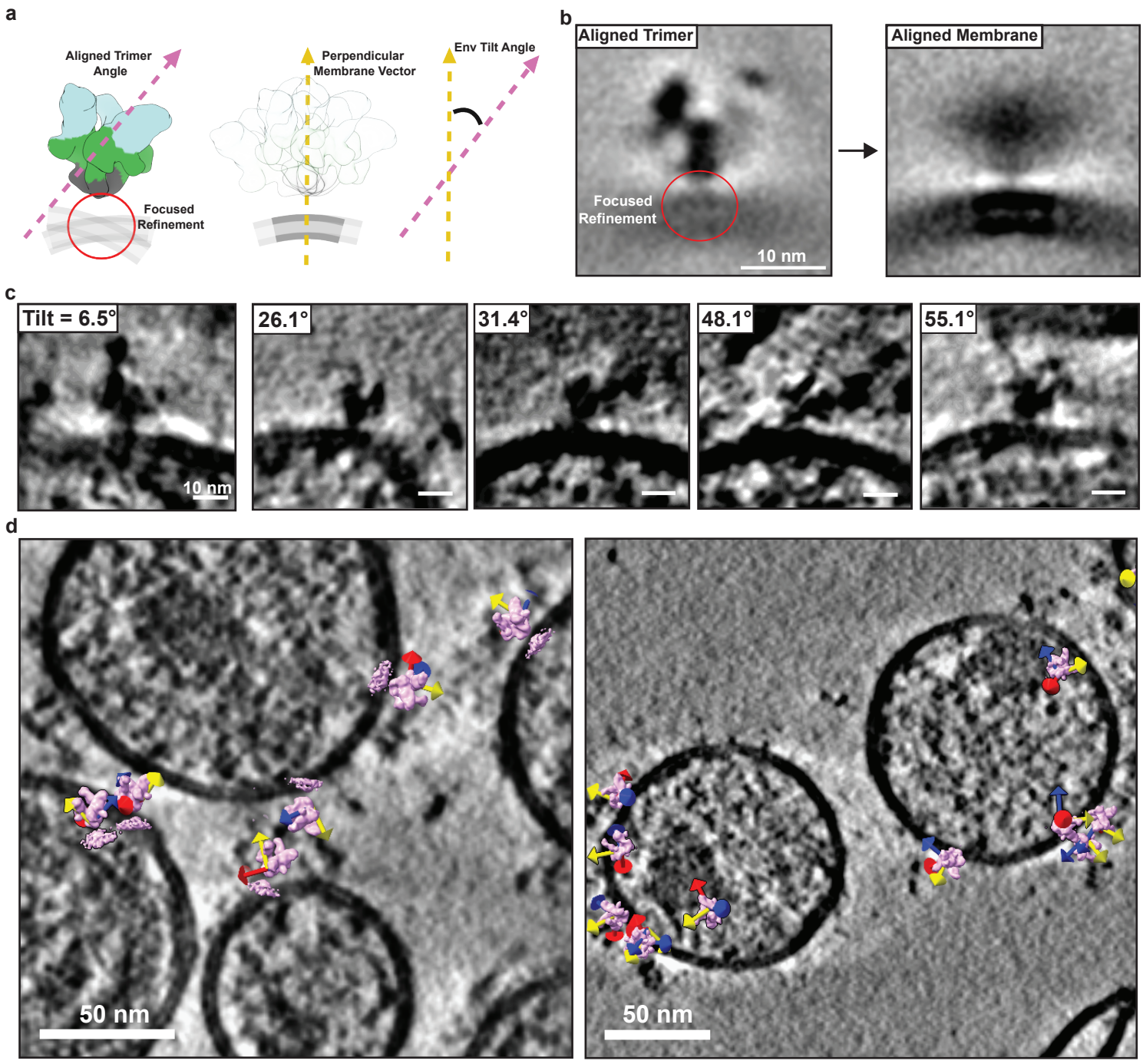

Supplementary Figure 14. Determination of per-particle Env tilting on the membrane. a, Cartoon schematic showing the calculation of Env tilting on the membrane. A perpendicular membrane vector (yellow) is determined through focused angular refinement on the disordered membrane. The Env tilt angle is calculated as the angle between this vector and the vector along the axis of the refined trimer (pink). Cartoons were created in BioRender. Uchil, P. (2025) https://BioRender.com/x73q045. **b**, A central slice of the aligned average structure before (left) and after (right) focused membrane refinement. **c**, Tomographic slices of individual particles with shown calculated tilt angles. **d**, Orientations and positions before and after membrane refinement were mapped back to tomograms in ArtiaX for visualization. The pink trimer position and orientation represent particles of the aligned trimer structure. The positions and orientations after membrane refinement are represented by the three principal axes (red, blue, and yellow); the yellow axis indicates the perpendicular membrane vector.

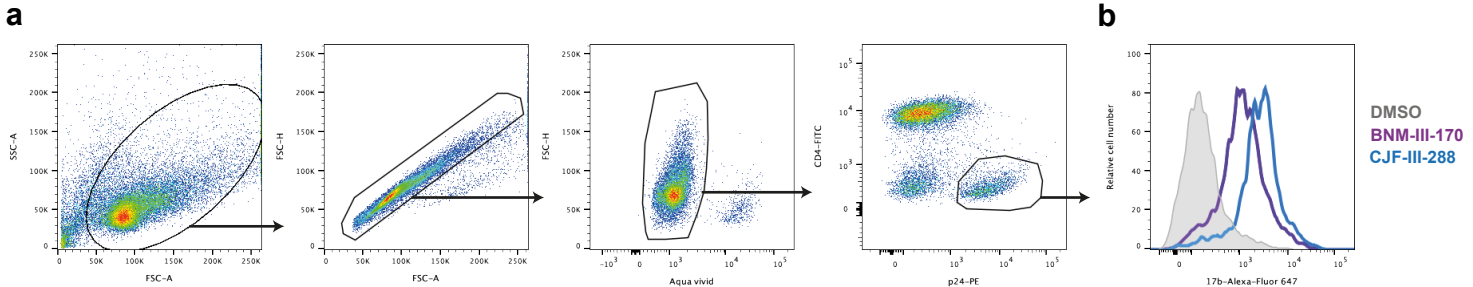

Supplementary Figure 15. Flow cytometry gating strategy for antibody binding. Representative gating strategy used to quantify mAb or plasma binding at the surface of HIV-1–infected cells. **a**, Infected cells were identified based on light-scatter parameters to define cell morphology, followed by exclusion of doublets and Aqua Vivid–positive dead cells, and gating on CD4lowp24+cells. **b**, Representative overlay histograms showing 17b binding in HIV-$1_{CH058TF}$-infected cells treated with DMSO, BNM-III-170 (1 μM), or CJF-III-288 (1 μM).

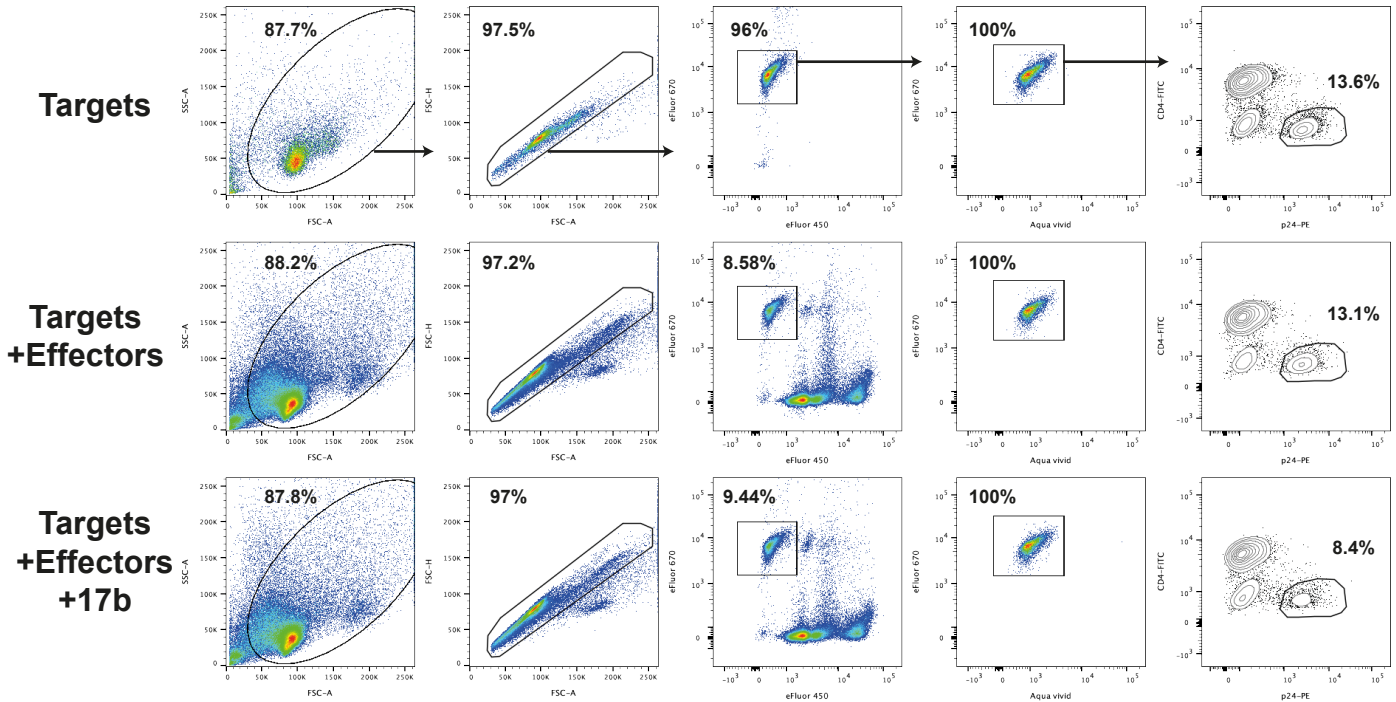

Supplementary Figure 16. Flow cytometry gating strategy for the ADCC assay. Representative gating strategy used to quantify ADCC responses against HIV-1–infected cells. Infected cells were first identified by light-scatter parameters to define cell morphology, followed by doublet exclusion. Gating was then performed on eFluor 670+ cells, excluding Aqua Vivid–positive dead cells, and selecting CD4lowp24+ cells. Shown are representative plots from an experiment performed with HIV-$1_{CH058TF}$-infected cells in the presence of CJF-III-288 (1 μM).